# Synthesis and DNA Interactions of Benzimidazole Dications Which Have Activity against Opportunistic Infections

Richard L. Lombardy,[†] Farial A. Tanious,[†] Kishore Ramachandran,[‡] Richard R. Tidwell,[‡] and W. David Wilson*[,†]

*Department of Chemistry, Georgia State University, Atlanta, Georgia 30303, and Department of Pathology, University of North Carolina, Chapel Hill, North Carolina 27599*

*Received October 27, 1995*[⊗]

Considerable evidence now indicates that DNA is the receptor site for dicationic benzimidazole anti-opportunistic infections agents (Bell, C. A.; Dykstra, C. C.; Naiman, N. A. I.; Cory, M.; Fairley, T. A.; Tidwell, R. R. *Antimicrob. Agents Chemother.* **1993**, *37*, 2668−2673. Tidwell, R. R.; Jones, S. K.; Naiman, N. A.; Berger, I. C.; Brake, W. R.; Dykstra, C. C.; Hall, J. E. *Antimicrob. Agents Chemother.* **1993**, *37*, 1713−1716). To obtain additional information on benzimidazole−receptor complexes, the syntheses and DNA interactions of series of symmetric benzimidazole cations, linked by alkyl or alkenyl groups, have been evaluated. Biophysical techniques, thermal denaturation measurement ($\Delta T_m$), kinetics, and circular dichroism (CD) have been used in conjunction with NMR and molecular modeling to evaluate the affinities, binding mode, and structure of complexes formed between these compounds and DNA. All of the compounds bind strongly to DNA samples with four or more consecutive AT base pairs, and they bind negligibly to GC rich DNA or to RNA. Spectral and kinetics characteristics of the benzimidazole complexes indicate that the compounds bind in the DNA minor groove at AT sequences. NMR and molecular modeling of the complex formed between an ethylene-linked benzimidazole derivative, **5**, and the self-complementary oligomer d(GCGAATTCGC) have been used to establish structural details for the minor groove complex. These results have been used as a starting point for molecular mechanics calculations to refine the model of the minor groove−benzimidazole complex and to draw conclusions regarding the molecular basis for the effects of substituent changes on benzimidazole−DNA affinities.

## Introduction

Organic cations that bind noncovalently in the minor groove of DNA generally fall into two classes: (i) alkyl-linked amines (such as spermine and spermidine) that bind tightly at low ionic strength but with limited specificity and (ii) extended conjugated systems with unfused aromatic rings that are directly bonded (such as DAPI, Hoechst 33258, furamidine) or are connected through conjugated systems (such as netropsin, distamycin, berenil, and stilbamidine).[1−10] Structures of some of these compounds are compared in Chart 1.

The aromatic amidine, pentamidine (Chart 1), which is being used clinically against *Pneumocystis carinii* pneumonia (PCP), the most common and leading cause of morbidity and mortality in AIDS patients,[11,12] is a different type structure with the aromatic groups linked through an alkyl chain. The mechanism of action of pentamidine and derivatives is believed to involve formation of a complex with the DNA of the microorganism, followed by selective inhibition of a DNA interactive microbial enzyme. There is now considerable evidence that the enzyme inhibited by the pentamidine−DNA complex is topoisomerase II of *Pneumocystis*,[13−15] and this inhibition rapidly leads to cell death.

Pentamidine binds relatively weakly in the DNA minor groove in AT sequences[16,17] and shows some side effects that limit its drug use.[14] We are involved in the design, synthesis, and study of minor groove binding cations with the goal of improving efficacy by enhancing specific DNA binding interactions and microbial enzyme inhibition selectivity.[18−20] Alkyl-linked benzimidazoles (Table 1) show improved anti-PCP activity and decreased toxicity relative to pentamidine.[20] Initial studies indicate that the compounds interact with DNA more strongly than pentamidine and inhibit the topoisomerase II enzyme of the microorganism to give the observed biological activity.[13,21] We report here a comparative study of the binding strength, kinetics, and binding mode of a variety of alkyl-linked benzimidazoles. These studies are essential for establishing the biological mode of action of these compounds and they form the basis of design experiments for the next generation of synthetic anti-PCP agents. Compound **6** of Table 1 is in preliminary clinical trials against PCP.

## Chemistry

The starting reagents for the bisbenzimidazoles **8**−**10** are the appropriate diamine **13a** or **13b**, which can readily be prepared according to reported procedures.[17,18] Reaction of **13a** or **13b** with (**14a**) under oxidative conditions in refluxing ethanol[22] provided the *N*-acetamidobisbenzimidazoles (**15a** or **15b**). The reaction proceeds readily and purification is straightforward. Deacetylation in 2 N HCl followed by reduction of the nitro group with catalytic hydrogenation provided the diamine **17a** and **17b**. All the intermediates were fully characterized by $^1$H NMR and microanalysis as described in the Experimental Section. The final step in the preparation of compounds **8**−**10** was first attempted using the Pinner synthesis.[23] Reactions of the imidates prepared from succinonitrile or 1,4-dicyanobutane with **17a** or **17b** were not successful in achieving the desired coupling reaction. The problem could be attributed to

[†] Georgia State University.
[‡] University of North Carolina.
[⊗] Abstract published in *Advance ACS Abstracts,* March 1, 1996.

0022-2623/96/1839-1452$12.00/0 

**Chart 1**

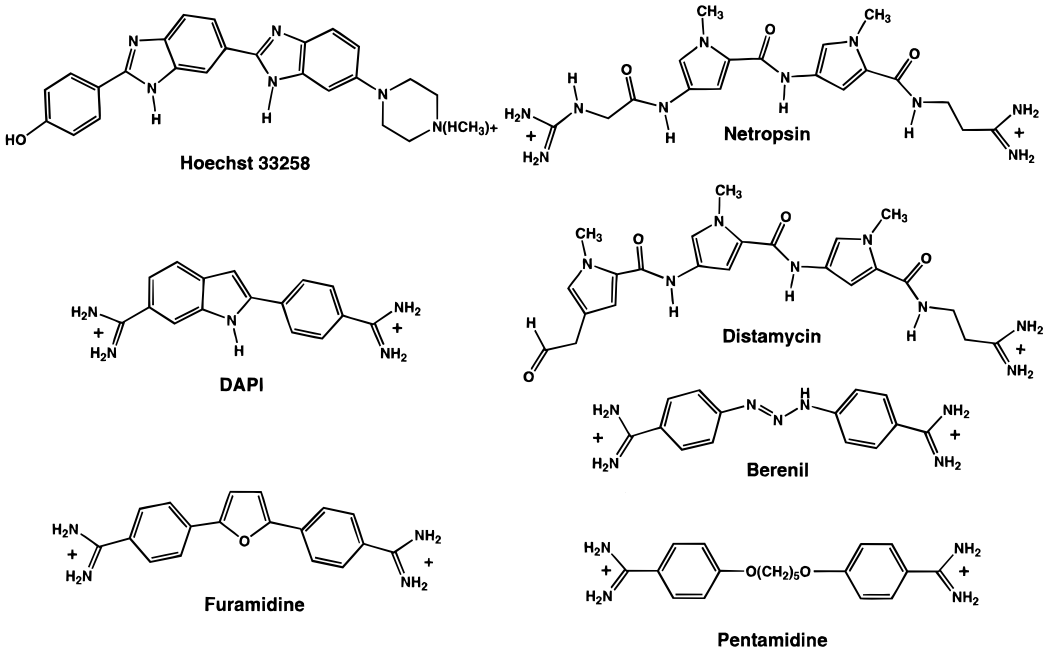


**Table 1.** Nucleic Acid Binding

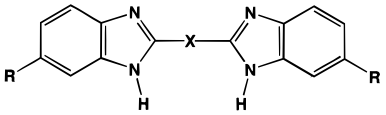

| Compound | X | R | ΔTm polydA.polydT | ΔTm polyA.polyU | ΔTm d(CGCGAATTCGCG)$_2$ | ΔTm d(G-C)$_4$ | K d(CGCGAATTCGCG)$_2$ |
|---|---|---|---|---|---|---|---|
| Pentamidine | | | 12.8 | 0 | 4.8 | 0 | $2.3\times10^6$ |
| DAPI | | | >26 | 3.9 | 22.2 | 2.5 | $4.5\times10^8$ |
| 1 | -C≡C- | Am | >26 | 0 | 22.8 | -1.5 | $5.3\times10^8$ |
| 2 | $(CH_2)$ | Am | 4.9 | -0.8 | 2.8 | 0 | $9.3\times10^5$ |
| 3 | $(CH_2)$ | Im | 5.7 | -0.6 | 2.8 | 0 | $9.3\times10^5$ |
| 4 | $(CH_2)_2$ | Am | >26 | -1.1 | 15.9 | 0.75 | $7.6\times10^7$ |
| 5 | $(CH_2)_2$ | Im | >26 | 0.9 | 16.4 | 0.70 | $8.8\times10^7$ |
| 6 | $(CH_2)_4$ | Am | 24.4 | -0.6 | 10.0 | 0.50 | $1.3\times10^7$ |
| 7 | $(CH_2)_4$ | Im | 25.5 | -1.5 | 7.1 | 0.50 | $5.2\times10^6$ |
| 8 | $(CH_2)_2$ | BzIm | >26 | 0 | 28.5 | 0 | $2.0\times10^9$ |
| 9 | $(CH_2)_4$ | BzAm | >26 | 0 | 22.2 | 0 | $4.5\times10^8$ |
| 10 | $(CH_2)_4$ | BzIm | >26 | 0 | 20.8 | 0 | $3.1\times10^8$ |

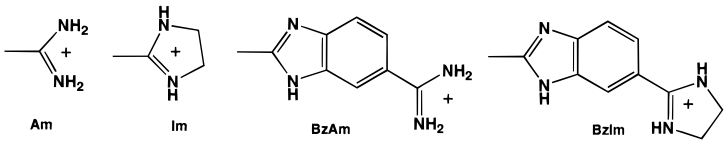


the insolubility of the diamines in appropriate organic solvents including glacial acetic acid, which is the standard solvent used for the coupling of imidates with diamines to give the desired imidazoles. The reaction of either **17a** or **17b** with succinic acid or adipic acid in 4 N HCl was carried out using a method described by Phillips.[24] The reaction, monitored by HPLC, required 1 week of reflux for gradual conversion of the diamine to the desired product. The reaction appears to progress through the intermediate *o*-aminoanilide.[25,26] When the reaction is complete, the aqueous solution is concentrated, and the residue purified by repeated recrystallization from ethanol to provide the desired products.

## Binding Affinity and Specificity

Representative $T_m$ curves for the sequence d(CGCGAATTCGCG)$_2$ and its complexes with **1** and **5** are shown in Figure 1. Increasing the ratio of compound to duplex from 1 to 2 did not result in a significant additional increase in the complex $T_m$. The $\Delta T_m$ values ($T_m$ complex − $T_m$ DNA) cover a range of >20 °C for **1**−**10** with the weakest binding observed for **2** and **3**, intermediate binding for **6** and **7**, and very strong binding for the other compounds (Table 1). A larger magnitude but similar order of $\Delta T_m$ values is observed with the polymer poly(dA)·poly(dT), and the $T_m$ curves

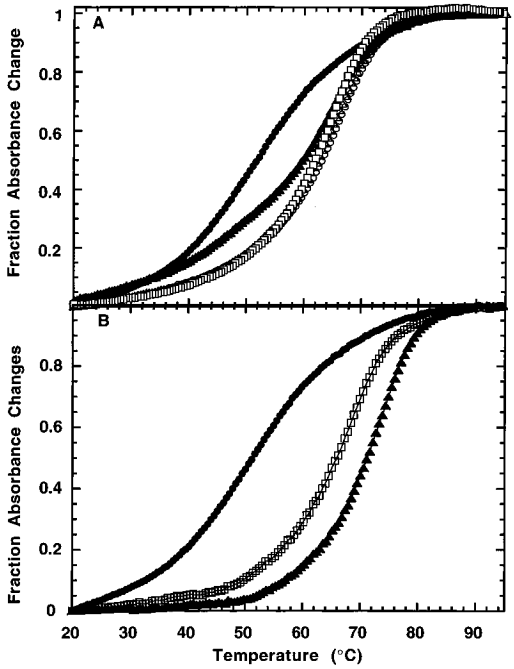


**Figure 1.** (A) The effect of **1** as a function of ratio on the melting curve of d(CGCGAATTCGCG)$_2$. Experiments were conducted in MES buffer with 0.1 M NaCl added; the concentration of d(CGCGAATTCGCG)$_2$ was $3 \times 10^{-6}$ in duplex and the molar ratio of compound/duplex were 0 (●), 0.5 (▲), 1.0 (△), 1.5 (○), and 2 (□). (B) Comparison of the effect of **1** (▲), and **5** (□) on the melting curve of d(CGCGAATTCGCG)$_2$ (●). Experiments were conducted in MES buffer with 0.1 M NaCl added, the concentration of d(CGCGAATTCGCG)$_2$ was $3 \times 10^{-6}$ in duplex, and the molar ratio of compound/duplex was 1.0.

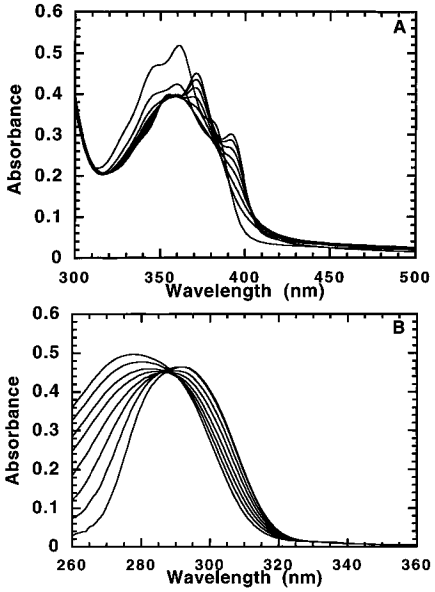


**Figure 2.** Spectrophotometric titrations of compound **1** (A), and compound **5** (B) with d(CGCGAATTCGCG)$_2$. Titrations were conducted in 1 cm cell in MES buffer with 0.2 M NaCl added at 25 °C. (A) The concentrations are as follows: $3 \times 10^{-5}$ M of compound **1**, and d(CGCGAATTCGCG)$_2$ concentrations in duplex of zero, $9.20 \times 10^{-7}$, $1.83 \times 10^{-6}$, $2.74 \times 10^{-6}$, $3.65 \times 10^{-6}$, $4.55 \times 10^{-6}$, $5.44 \times 10^{-6}$, and $6.33 \times 10^{-6}$, respectively, from the top to the bottom curves at 360 nm. (B) The concentrations are as follows: $2 \times 10^{-5}$ M of compound **5**, and d(CGCGAATTCGCG)$_2$ concentrations in duplex of zero, $3.07 \times 10^{-6}$, $6.08 \times 10^{-6}$, $9.03 \times 10^{-6}$, $1.19 \times 10^{-5}$, $1.48 \times 10^{-5}$, $1.76 \times 10^{-5}$, and $2.03 \times 10^{-5}$, respectively, from the top to the bottom curves at 275 nm.

for complexes of **1**, **4**, **5**, and **8**−**10** are shifted to greater than 95 °C. Melting experiments were also conducted with the corresponding sequence RNA polymer, poly(A)·poly(U), but no significant $T_m$ increase was observed for the RNA sequence with any of the benzimidazoles. A similar lack of $T_m$ increase with **1**−**10** is observed with the GC base pair duplex formed by sequence d(GCGCGCGC)$_2$. These results agree with those of Bell et al.[13] for melting of AT and GC polymer DNA samples with compounds **1**−**7** at low salt concentrations. Results for the aromatic diamidines pentamidine and DAPI, which have been crystallized in complex with the oligomer d(CGCGAATTCGCG)$_2$, are shown in Table 1 for comparison.

Spectral changes on addition of d(CGCGAATTCGCG)$_2$ to **1** are shown in Figure 2A. In the initial stages of the titration at high ratios of **1** to duplex, there is a large decrease in absorbance with little shift in wavelength. On continued addition of oligomer duplex there is a gradual shift to longer wavelength, and a limiting complex spectrum is reached near a ratio of one compound per duplex. This spectral behavior along with the $T_m$ results suggests that, up to a ratio of one compound per duplex, the compound is bound only at the strong AATT binding site. At higher ratios weaker binding of the compound, probably primarily by electrostatic interactions, is observed. The observed spectral changes and extended conjugated system of **1** both supported this dual type of binding process.

A similar titration of **5** with the oligomer duplex is shown in Figure 2B. The wavelength maximum of **5** is shifted to lower wavelength as with all of the derivatives **2**−**6** (not shown) which do not have an extended conjugated system as in **1**. The spectrum of **5** significantly overlaps that of the DNA bases, but Figure 2B is a difference spectrum obtained by subtraction of DNA absorbance. Compound **5** does not have the initial aggregation-induced absorbance drop observed with **1** (Figure 2A), but shows a gradual shift to longer wavelength and slight decrease in extinction coefficient on titration with DNA. A clear isosbestic point is not obtained in the titration, but this could be due to slight errors in subtraction of the large DNA absorbances. The low absorbance wavelengths of **2**−**7** and the duplex-induced aggregation problems of **1** prevent direct calculation of binding equilibrium constants from the spectral results, and we have turned to other methods to evaluate binding constants.

The results of an ethidium displacement assay with complexes of **1**−**10** with polyd(A-T)$_2$ are in general agreement with the results from $T_m$ studies (Figure 3). The highest concentration required for 50% displacement of ethidium is observed with **2**, and this is followed closely by **3** (Figure 3). Intermediate, but much lower, concentrations of **6** and **7** are required for ethidium displacement while **1**, **4**, **5**, and **8**−**10** require the lowest concentrations for displacement. Although a number of assumptions are involved in calculation of binding constants by displacement of the intercalator ethidium by these compounds, it is clear that the binding constants of **1** and **4**−**10** are predicted to be greater than $10^7$ under these conditions while the binding constants of **2** and **3** are close to $10^6$. The conclusion from all of these results is that **1** and **4**−**10** bind very strongly to AT sequences and much more weakly to GC sequences

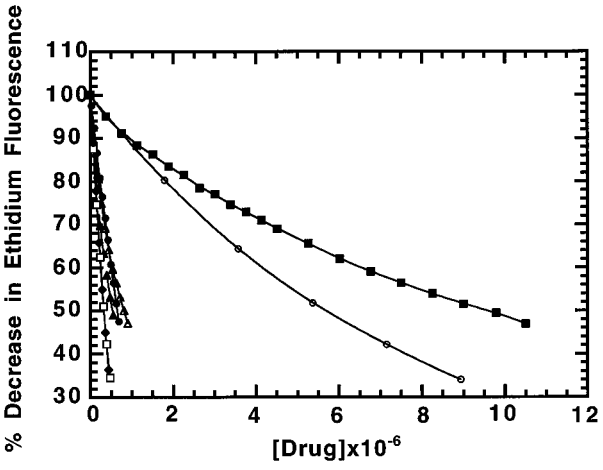


**Figure 3.** The decrease in ethidium fluorescence at 596 nm (excitation at 546 nm) of a complex of ethidium and polyd(A-T)$_2$ on addition of various concentrations of compounds **1** (●), **2** (■), **3** (○), **4** (◆), **5** (□), **6** (▲), and **7** (△).

in DNA or to any sequence in RNA. The order of binding of **1**−**10** to AT sequences is **1** > **8**−**10** > **4**, **5** > **6**, **7** ≫ **2**, **3**.

From the $\Delta T_m$ values for all bisbenzimidazoles compounds complexed with d(CGCGAATTCGCG)$_2$, binding constants were calculated by method of Crothers[27] according to the equation shown below, and the results are shown in Table 1

$$1/T_m° - 1/T_m = R/\Delta H° \ln(1 + Ka_L) = \Delta T_m/T_m \cdot T_m°$$

where $T_m°$ is the melting temperature of the free DNA, $\Delta H°$ is the enthalpy of melting for the free DNA, $T_m$ is the melting temperature of the complex, $K$ is the binding equilibrium constant, and $a_L$ is the free ligand concentration.

### Binding Kinetics

Both UV−visible and fluorescence spectral changes can be used to monitor the kinetics of binding. A plot of fluorescence spectral changes as a function of time for dissociation of a **1**−polyd(A-T)$_2$ complex as an example is shown in Figure 4. Two exponential fits to the data are also shown along with plots of residuals. Single exponential fits give unsatisfactory residuals and significantly higher RMS deviations with all the complexes of these compounds with the polymer. Three exponential fits do not significantly improve the residuals or RMS deviations.

For the purposes of comparison, the dissociation lifetime ($\tau$) and apparent rate constant ($k_{app} = 1/\tau$) were calculated from the computer-derived, best-fit values for rate constants and amplitudes:

$$\tau = 1/(A_1k_1 + A_2k_2)$$

where $A$ and $k$ values refer to the amplitudes and rate constants for the two exponential fits to the dissociation results. Plots of the dissociation rate constants for complexes of **1**, **4**, **5**, and **7** determined as in Figure 4 are shown in Figure 5 as a function of log [Na$^+$] at constant temperature. The slopes of the plots are all 1.7 ± 0.1 in agreement with the slope obtained for the DAPI−polyd(A-T)$_2$ complex[4,28] (Figure 5).

The association of **1** with polyd(A-T)$_2$ was also followed by stopped-flow methods (Figure 6), but the

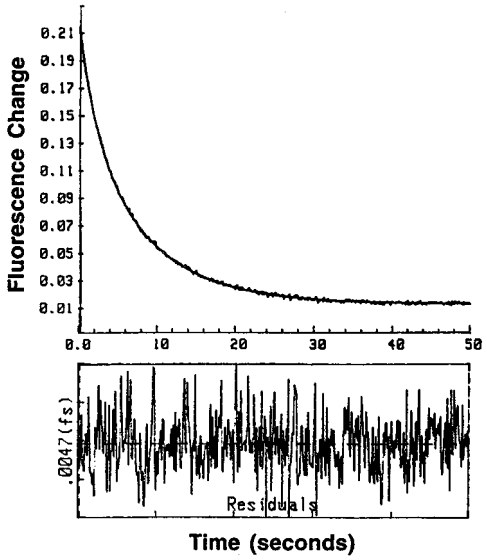


**Figure 4.** Stopped-flow kinetics traces for the SDS-driven dissociation of compound **1** with polyd(A-T)$_2$. The experiments were conducted at 20 °C in MES buffer with [Na$^+$] = 0.135 M at a ratio of 1:10 compound to polymer base pairs. The concentration of compound **1** after mixing was $1.0 \times 10^{-6}$ M. The smooth lines in the panels are the two exponential fits to the experimental data. Residual plots are shown under the experimental plot.

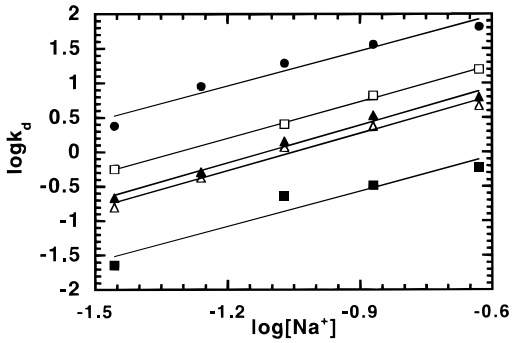


**Figure 5.** Plots of log $k_{app}$ vs −log [Na$^+$] for dissociation from polyd(A-T)$_2$ of **1** (■), **4** (▲), **5** (△), **7** (●), and DAPI (□). Experiments were conducted in MES buffer at different ionic strengths in the manner described in Figure 4.

fluorescence spectral signals for **2**−**7** are not satisfactory for experiments at the low concentrations required to measure association by stopped-flow techniques. The association results are plotted in Figure 7 as a function of salt concentration. Results for DAPI, the dicationic intercalator propidium, and a naphthalenediimide that binds by a threading intercalation mode are included in Figure 7 for reference. As with the dicationic diamidine DAPI, **1** binds to AT sequence in DNA with a $k_a > 10^7$ M$^{-1}$ s$^{-1}$ that does not vary with the salt concentration as extensively as with the intercalators. The calculated equilibrium constant for **1** with a $k_a$ of $>10^7$ M$^{-1}$ s$^{-1}$ and a $k_d$ of ∼0.1 s$^{-1}$ at 0.1 M Na$^+$ is $>10^8$ M$^{-1}$, in agreement with the high values calculated from the $T_m$ studies (Table 1).

All of benzimidazoles have similar slopes for their dissociation constants, and if they have similar association rate constants, close to the diffusion-limit value, the calculated equilibrium constants from the association and dissociation kinetics results are 5−10 times lower for **4** and **5** than for **1** while **6** and **2** have binding

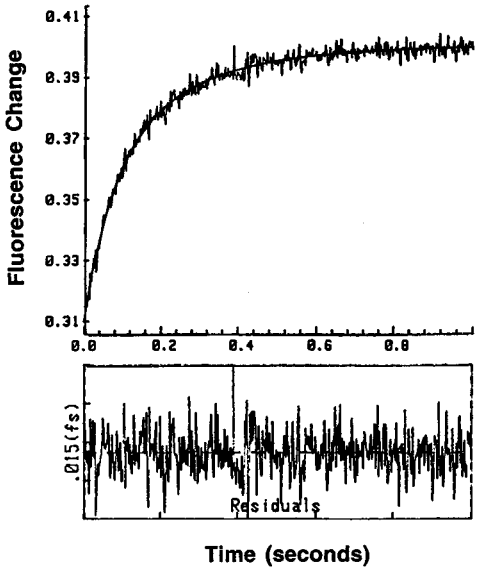


**Figure 6.** Stopped-flow kinetics traces for the association of compound **1** with polyd(A-T)$_2$. The experiments were conducted at 20 °C in MES buffer with [$Na^+$] = 0.319 M at a ratio of 1:10 compound to polymer base pairs. The concentration of compound **1** was $2.5 \times 10^{-8}$ M and the DNA was $2.5 \times 10^{-7}$ M in base pairs after mixing. The smooth lines in the panels are the two exponential fits to the experimental data. Residual plots are shown under the experimental plot.

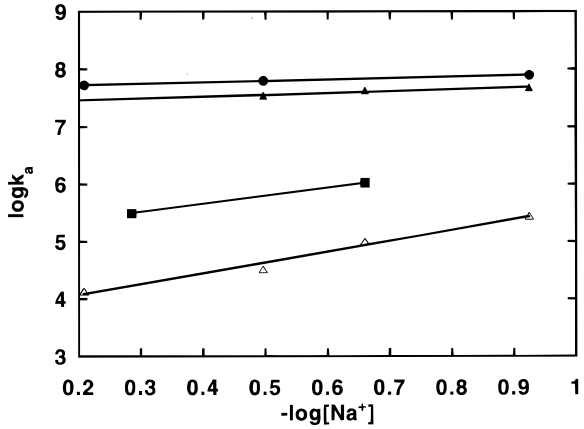


**Figure 7.** Plots of log $k_{app}$ vs −log [$Na^+$] for association of **1** (▲) with polyd(A-T)$_2$, propidium with CTDNA (■), naphthalene diimide with polyd(C-G)$_2$ (△), and DAPI with polyd(A-T)$_2$ (●). Experiments were conducted in MES buffer at different ionic strengths in the manner described in Figure 6.

constants that are 50−100 times lower than for **1** in agreement with the calculated equilibrium constants in (Table 1).

## CD Spectra

CD spectra were obtained for benzimidazole complexes in both the wavelength region above 300 nm, where DNA does not absorb and all bands are due to induced CD in bound compounds, and the region below 300 nm, where both DNA and the compounds absorb (Figure 8A−D). None of the benzimidazoles derivatives has an intrinsic CD spectrum. Addition of compound **1** to polyd(A-T)$_2$ in 0.1 M NaCl results in a small decrease of the DNA signal at 260 nm, increase in the DNA signal at 230 nm, and a strong positive CD signal at 375 and 395 nm (Figure 8A). Addition of compound **2** to polyd(A-T)$_2$ results in a very weak CD signal at 295 and no change in the DNA signal in 0.1 M NaCl (not shown).

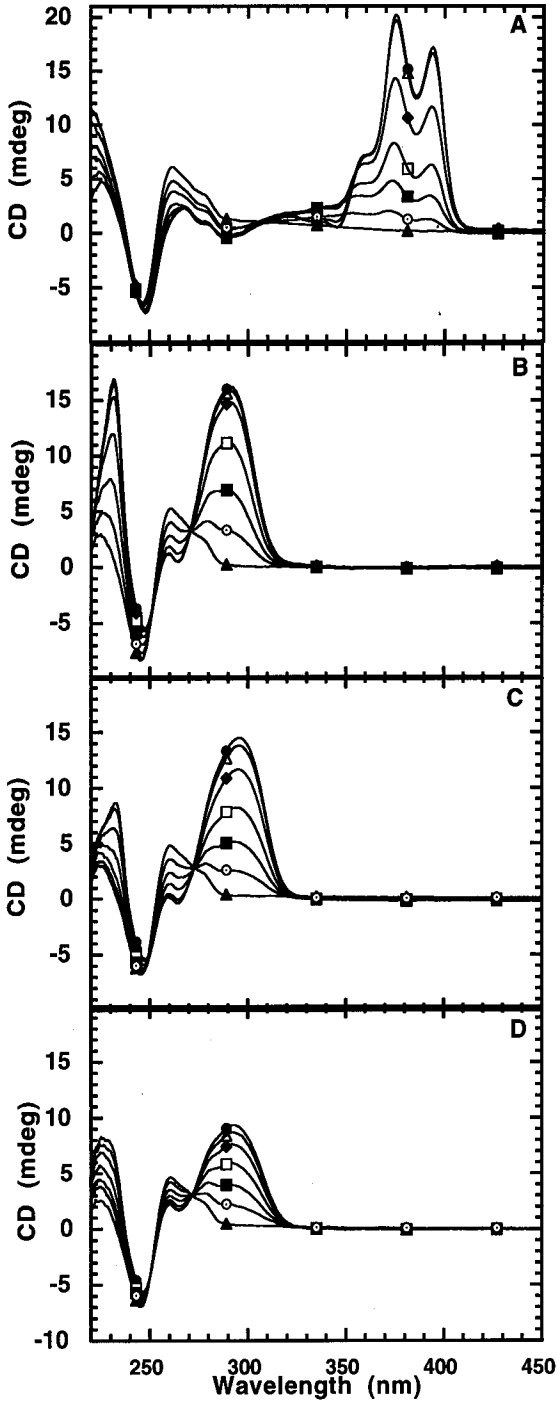


**Figure 8.** CD spectra of compounds **1** (A), **4** (B), **5** (C), and **7** (D) with polyd(A-T)$_2$. Experiments were conducted in a 1 cm cell in MES buffer with 0.1 M NaCl added at 25 °C. The ratio of compound/polymer in base pairs is 0 (▲), 0.05 (○), 0.10 (■), 0.15 (□), 0.20 (◆), 0.25 (△), and 0.3 (●).

Addition of compound **4** to polyd(A-T)$_2$ results in a decrease of the DNA signal at 260 nm, an increase in the DNA signal at 230 nm, a strong positive CD signal at 290 nm, and very clear isoeleptic points at 270 and 250 nm. The CD results for complex with **5** are very similar to those with **4**. The only significant difference between the two results is that the increase in the DNA signal at 230 nm is less with compound **5** (Figure 8B,C). Addition of **7** to polyd(A-T)$_2$ results in a decrease in the DNA signal at 260 nm, a strong positive CD signal at 290 nm, and very clear isoeleptic points at 270 and 250 nm (Figure 8D). The induced signal at 290 nm is less

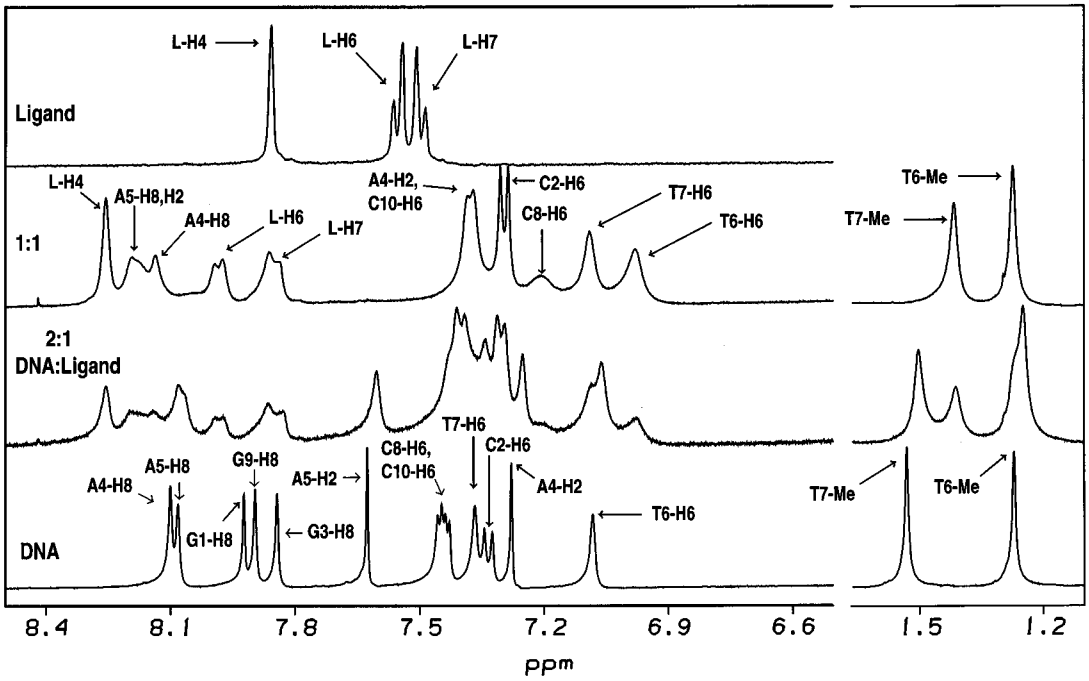


**Figure 9.** The aromatic and thymine methyl regions of the spectra for the titration of compound **5** into DNA are shown. For the two ratios of the complex the guanine H8 protons were exchanged with deuterium to simplify the spectrum.

for **7** than **5** at the same ratio in agreement with the observed greater binding constant for **5**.

## NMR

To obtain additional structural information on the benzimidazole−DNA complexes, NMR spectra of **5** complexed with d(GCGAATTCGC)$_2$ were obtained. The chemical shifts of the nonexchangeable protons were assigned through a combination of 1D titration spectra, as well as NOESY and COSY 2D experiments. For the free DNA, the chemical shift assignments of the nonexchangeable protons have been reported.[29−31] In the 1D titrations at 35 °C (Figure 9) major downfield shifts are seen for A5-H2 and the aromatic protons of **5**, while large upfield shifts are seen for the H6 and H1′ of T7. The change in chemical shifts upon binding the ligand for several protons along the duplex are plotted in Figure 10, and it can be seen that the most dramatic changes occur in the central AT rich region. The spectrum at a 2:1 ratio of DNA to ligand (Figure 9) contains resonances from both the free DNA and the DNA−ligand complex, indicating that the complex is in slow exchange with free DNA on the NMR time scale. Figure 11 contains plots of the aromatic region of the NMR spectrum for the 1:1 complex at temperatures ranging from 5 to 60 °C. At low temperature, substantial line-broadening occurs. This can be attributed to exchange between different species and is probably due to the sliding motion of the drug along the DNA. Above 25 °C the signals are sharper and the bound species in the complex are in fast exchange. The H8/H6 to H1′ region of the 2D NOESY spectrum for the 1:1 complex is shown in Figure 12. This plot also shows one of the strong cross peaks between the ligand (H4) and DNA (A5-H2) while the other two strong cross peaks, L-H4 to A5-H1′ and L-H4 to T7-H1′, are shown in Figure 13.

## Molecular Modeling

On the basis of the X-ray structure of pentamidine bound to d(GCGAATTCGC)$_2$ and the NMR structural

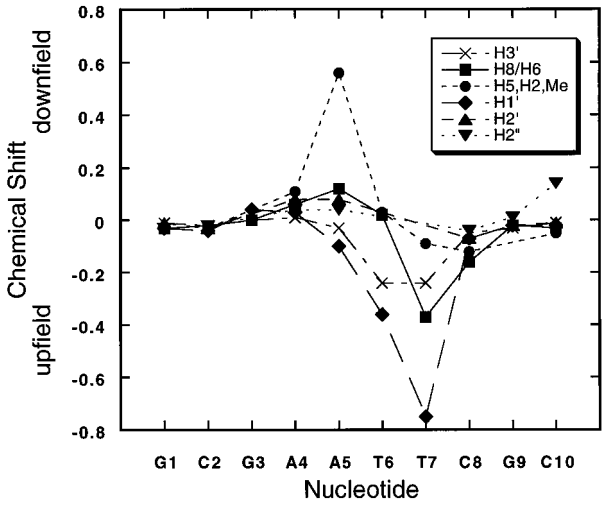


**Figure 10.** The change in chemical shift upon ligand binding (complex-free) for the assigned protons of the DNA is shown. H8, H6 (■); H5, H2, Me (●); H1′ (◆); H2′ (▲); H2″ (▼); H3′ (×).

data described above, a model of the decamer complexed to **5** was built, and energy minimized as described in the Methods Section (Figure 14). The compound binds at the central AT region with the bound ligand spanning five base pairs. The model indicates that a number of hydrogen bonds between the ligand and DNA are possible. These can occur between the imidazole NH group and T17-O2 (2.7 Å), A4-N3 (2.9 Å), and A5-N3 (3.8 Å), and between the benzimidazole NH group and T16-O2 (1.9 Å), T17-O2 (3.8 Å), T6-O2 (3.2 Å), and A5-N3 (3.9 Å) at one end of the ligand. At the other end of **5** in the complex the imidazole NH can hydrogen bond with T7-O2 (2.0 Å) and A14-N3 (3.1 Å) while the benzimidazole NH can hydrogen bond with T7-O2 (1.9 Å) and A15-N3 (3.1 Å). The imidazole NH at this end of the molecule is only 2.0 Å away from the O2 of C8 while the corresponding distance at the other end of the molecule with C18−O2 is 3.9 Å. This difference and

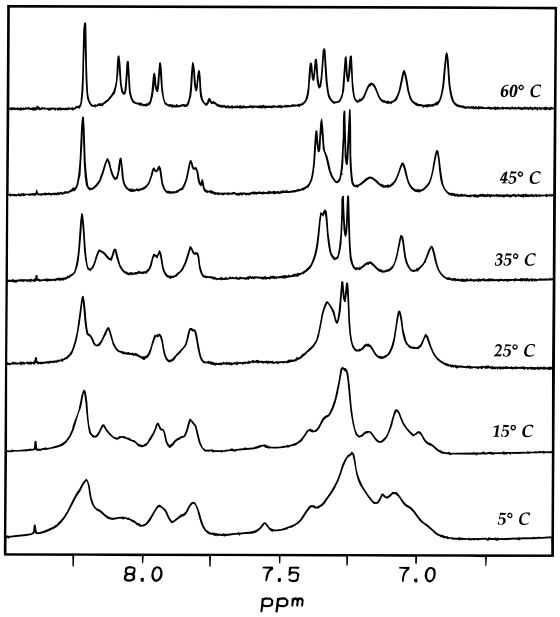


**Figure 11.** The aromatic region of the spectra for the 1:1 complex of compound **5** with the decamer are shown at temperatures ranging from 5 °C to 60 °C.

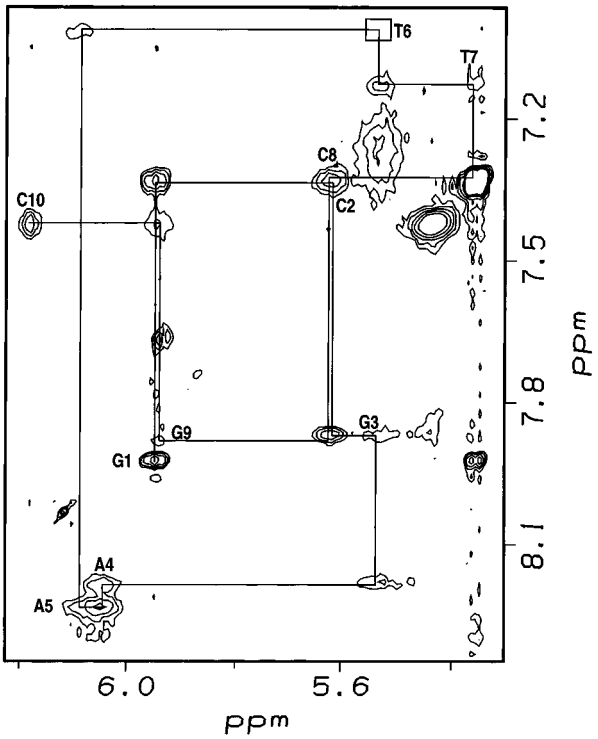


**Figure 12.** The aromatic to H1′ cross peak region of the 350 ms NOESY spectrum at 35 °C is shown. The cross peak between the H6 and H1′ of thymine 6 was not resolved, and its position is indicated by a box.

differences in the above hydrogen bond distances, point out the unsymmetrical nature of the model. The ligand can bind at two nearly symmetric sites spanning G3-T7 and A4-C8, and exchange between these sites may explain the broadened, more complicated NMR spectra observed for the 1:1 complex at low temperature.

## Discussion

The $T_m$ studies conducted as a function of ratio indicate that the benzimidazoles of Table 1 have a single, strong binding site on the oligomer duplex

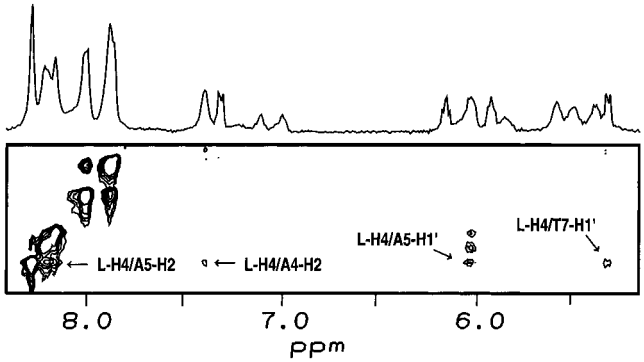


**Figure 13.** The cross peaks between the H4 of compound **5** and DNA from the 350 ms NOESY are shown. The *x*-axis range is from 8.4 to 7.8 ppm. The cross peak to A4-H2 is the weakest.

d(CGCGAATTCGCG)$_2$ as observed with a number of minor groove binding agents such as DAPI and pentamidine.[16,32] The compounds bind very strongly to DNA in extended sequences of AT base pairs but bind very poorly to DNA GC rich sequences and to RNA. These results are all characteristic of a minor groove binding mode,[3−5] and this binding mode for the benzimidazoles is confirmed by results from CD, kinetics, and NMR experiments.

Minor groove binding, for example, is characterized by relatively large association rate constants with much lower dissociation rate constants. The association rate constants have a very low dependence on salt concentration, while the dissociation rate constants have high dependence on salt concentration[33] and this is observed with the benzimidazoles (Figures 4−7). In addition, the NMR NOESY intermolecular cross peaks between **5** and the DNA oligomer duplex d(GCGAATTCGC)$_2$ are all to minor groove protons on AT base pairs (for example, to AH2 and to H1′ protons of A and T). The NMR cross peaks and X-ray structure of pentamidine were used as guides to dock **5** into the AATT minor groove binding site of the oligomer duplex, and the structure was energy minimized with the NMR intermolecular constraints. A final model was then obtained by energy minimization of the structure with all constraints removed (Figure 14). The model generated for the complex has the expected features of minor groove interactions.[19] The imidazole−benzimidazoles units slide deeply into the groove and their NH groups at the floor of the groove form hydrogen bonds to TO2 and AN3 acceptor groups. Specificity is generated by the tight fit of the benzimidazoles at the edge of the AT base pairs that would be completely disrupted by the 2-$NH_2$ group of G in a GC base pair.

The NMR spectra show a single set of NMR signals at temperatures above 30 °C, but become broader and more complex at lower temperatures. This result suggests that the benzimidazoles may have two (or more) binding sites that are in fast exchange above 30 °C but move into intermediate exchange below 30 °C. The broad peaks down to 0 °C preclude analysis of the spectra in the 0−30 °C region, but the molecular modeling results indicate that in the preferred binding mode **5** is not symmetrically placed in the AATT binding sites of the d(GCGAATTCGC)$_2$ duplex. Each end of the AATT site could provide an identical binding environment, and the broadening at low temperature may represent slow exchange for sliding of the symmetrical

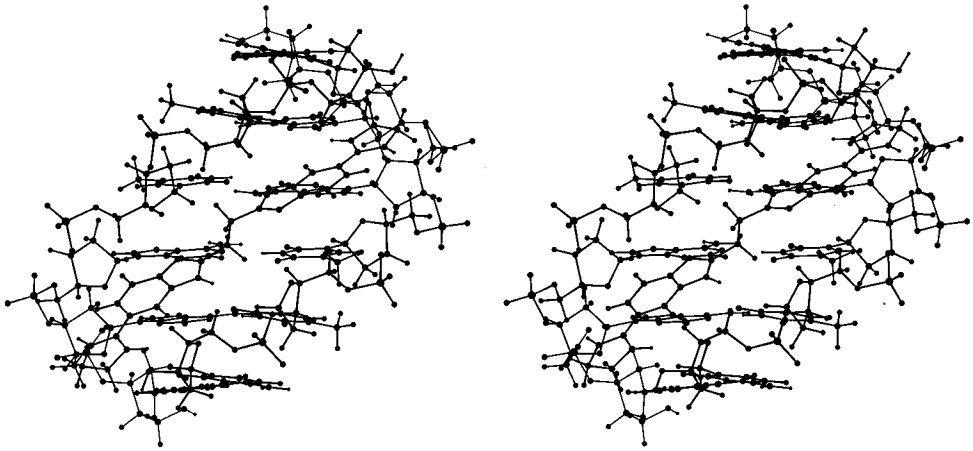

**Figure 14.** Stereoview of compound **5** bound to the central $(GAATTC)_2$ region of the decamer.

benzimidazole back and forth between the two symmetrical binding sites. Dissociation, rotation, and reassociation of benzimidazole would accomplish the same transformation.

This model correctly predicts the dramatic difference in interaction observed for the benzimidazoles derivatives at AT and GC sites in DNA as well as the observed difference for AT DNA and AU RNA binding sites. The minor groove base interaction chemistry for DNA and RNA is the same so that the benzimidazole could slide deeply into the RNA minor groove and hydrogen bond to AN3 and UO2 groups at the floor of the groove. The problem with this model is that in the A-form helical conformation of RNA the minor groove is not deep and narrow, as in AT sites in the B-form DNA, but wide and shallow.[34] The shift from a B-form to an A-form geometry thus destroys the structure and favorable electrostatics of the minor groove required for strong binding of compounds such as the benzimidazoles, netropsin, pentamidine, and related minor groove binding drugs.[1−10,16,17,28,32]

Finally, the model in Figure 14 can be used to interpret the binding constant differences observed as function of structure for the benzimidazole derivatives (Table 1). Compound **1** has a 5−10 times higher binding constant than **4**, and this is explained by the fit of the benzimidazoles into the narrow minor groove of AT sites in DNA. The more planar conjugated system of **1** fits better into the groove and makes better contacts with the walls of the groove than **4**. Compounds **4** and **5** with two methylene groups bind 5−10 times more strongly than **6** and **7** which have four methylene groups. The added methylenes of **6** and **7** do not form particularly favorable contacts with the minor groove in AT sequences, and there is a significant entropy loss on binding. This entropy loss, which results from the reduction in the multiple rotational configurations of **6** and **7** in solution to the much small number of configurations available for binding in the minor groove, accounts for the equilibrium constant reduction for **6** and **7** relative to **4** and **5**. It should be noted however, that even with **4** and **5** the binding constants are greater than $10^6$ $M^{-1}$ for AT sites under physiological relevant conditions.

The reason for the dramatic drop in binding for the single methylene compounds **2** and **3** is quite clear from the model. The tetrahedral geometry for the methylene group in **2** and **3** creates a significant angle between the two benzimidazoles that allows only one benzimidazole amidine/imidazoline group at a time to fit into the minor groove of DNA, and this results in a large decrease in interaction energetics. On the other hand, compounds with additional benzimidazole groups which can fit into the minor groove, **8**−**10**, have significantly enhanced binding with equilibrium association constants more than 20 times greater than those of corresponding bisbenzimidazoles.

It is interesting that enhanced binding of compounds such as **1** and **8**−**10** does not necessarily translate into better drugs. **1** and **8**−**10** have good activity, but they all display unacceptable toxicity with the PCP mouse model.[20] The very strong binding of these compounds may lead to binding at secondary sites that can cause toxicity. Compound **7** has a binding constant of $5 \times 10^6$ $M^{-1}$ at AATT sites, and this is obviously enough to give a strong cellular biological response. Future development in this series is focused on benzimidazoles that maintain this strong DNA binding, but which have enhanced DNA-associated enzyme inhibition that is responsible for the anti-PCP activity of this class of compounds.

## Experimental Section

Melting points are uncorrected and were measured on a Thomas Hoover capillary melting point apparatus or a Mel-Temp II apparatus. IR spectra were recorded in Nujol mull or KBr pellet on a Perkin-Elmer 1320 spectrophotometer. $^1H$ NMR spectra were recorded on a Bruker AC 300 MHz or a Varian XL 400 MHz spectrometer. All spectra were recorded in DMSO-$d^{25}$ unless specified otherwise. Anhydrous ethanol was distilled over Mg immediately prior to use. Reaction products were dried over $P_2O_5$ at 77 or 110 °C at 0.2 mmHg. Unless stated otherwise, reactions were monitored by TLC on silica or by reverse phase HPLC. HPLC chromatograms were recorded on a Hewlett-Packard 1090 chromatograph interfaced with a Hewlett-Packard 3396 integrator utilizing UV detection (230 nm). Chromatography was performed on a Dupont Zorbax Rx C8 column (4.6 mm × 25 cm). Mobile phases consisted of mixtures of acetonitrile (5−67.5% v/v) in water containing 10 mM tetramethylammonium chloride, 10 mM sodium heptanesulfonate, and 2.2 mM phosphoric acid. Electron impact mass spectra were recorded on a VG 70-SE, a VG 70-SEQ Hybrid, or a JMS 0−100 double focusing spectrometer. FAB mass spectra were recorded on a VG 70-SEQ Hybrid spectrometer (cesium ion gun, 30 kV). Microanalyses were performed by Atlantic Microlab, Norcross, GA. The synthesis and physical properties of bisbenzimidazoles **1**−**7** (Table 1) and diamines **13a** and **13b** (Scheme 1) have been described in previous communications.[17,18] Preparation of **14a** (Scheme 1) was carried out according to a reported procedure.[35]

**Scheme 1**[a]

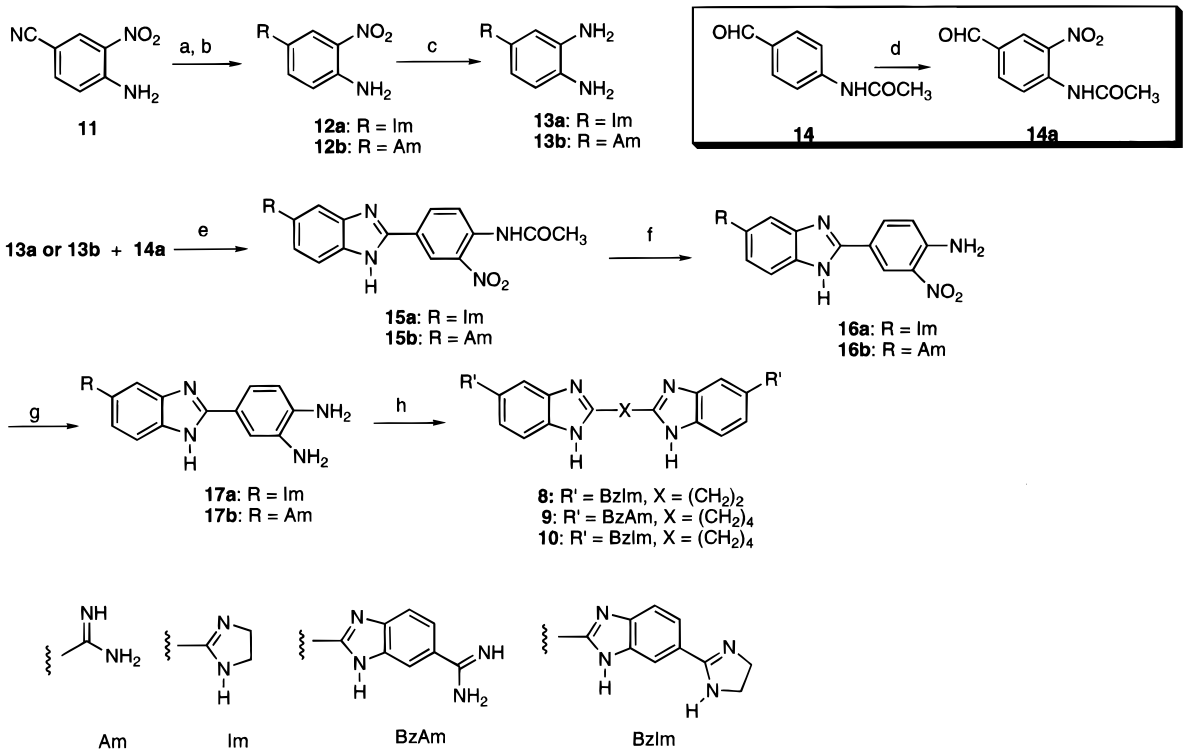


[a] Key: (a, b, c[2]); (d[8]); (e) 1,4-benzoquinone, ethanol, Δ, 4.5 h; (f) 2 N HCl, Δ, 2 h; (g) $H_2$, 10% Pd/C, MeOH, water, 1 h; (h) HOOC(X)COOH (where X = $(CH_2)_2$ or $(CH_2)_4$), 4 N HCl, Δ, 1 week.

**Preparation of 15a and 15b.** A mixture of the appropriate diamine (**13a** or **13b**, 5.0 mmol), 4-*N*-acetamido-3-nitrobenzaldehyde (**14a**, 5.0 mmol), and 1,4-benzoquinone (5.9 mmol) in ethanol (80.0 mL) was heated to reflux for 4.5 h. The flask was cooled in ice bath, and the solid that separated was filtered, washed with ethanol, and dried.

**2-(4-*N*-Acetamido-5-nitrophenyl)-5-imidazolinobenzimidazole (15a):** 1.8 g (90%); mp 240−242 °C; $^1$H NMR (ppm) 2.1 (s, 3 H), 4.02 (s, 4 H), 7.7−8.7 (m, 6 H), 10.65 (bs, 2 H), 14.11 (bs, 1 H). Anal. for $C_{18}H_{16}N_6O_3$·HCl, C, H, N.

**2-(4-*N*-Acetamido-5-nitrophenyl)-5-amidinobenzimidazole (15b):** 1.64 g (88%); mp 270−272 °C; $^1$H NMR (ppm) 2.13 (s, 3 H), 7.73−7.89 (m, 3H, $J$ = 8, 10 Hz), 8.26 (s, 1 H), 8.55 (s, 1 H), 8.78 (s, 1 H), 9.03 (s, 2 H), 9.34−9.39 (2s, 2 H), 10.64 (s, 1 H). Anal. for $C_{16}H_{14}N_6O_3$·HCl, C, H, N.

**Preparation of 16a and 16b.** The appropriate *N*-acetamidobenzimidazole (**15a** or **15b**, 14.25 mmol) in 2 N HCl (120 mL) was heated to reflux for 2 h. The solution was cooled in ice bath, and the solid that separated was filtered, washed with cold acetone, and dried to provide the appropriate nitro amine.

**2-(4-Amino-5-nitrophenyl)-5-imidazolinobenzimidazole (16a):** 4.9 g (96%); mp >325 °C; $^1$H NMR (ppm) 4.03 (s, 4 H), 7.25 (d, 1 H), 7.85 (d, 1 H), 7.96 (d, 1 H), 8.34−8.39 (m, 2 H), 9.01 (d, 1 H), 10.7 (s, 2 H). Anal. for $C_{16}H_{14}N_6O_2$·2HCl·2.5$H_2O$, C, H, N.

**2-(4-Amino-5-nitrophenyl)-5-amidinobenzimidazole (16b):** 5.0 g (87%); mp >325 °C; $^1$HNMR (ppm) 7.2 (d, $J$ = 9 Hz, 1 H), 7.77−7.87 (2d, 2 H, $J$ = 9 Hz), 8.18 (s, 1 H), 8.37−8.40 (m, 1 H), 9.05 (s, 1 H), 9.19 (s, 2 H), 9.50 (s, 2 H). Anal. for $C_{14}H_{16}N_6O_2$·2HCl·2$H_2O$, C, H, N.

**Preparation of 17a and 17b.** To the appropriate nitro amine (**16a** or **16b**, 3.01 mmol) dissolved in water (140 mL) was added 10% Pd/C (100 mg) and the solution hydrogenated at room temperature at 50 psi. The reaction was stopped after cessation of $H_2$ uptake. The catalyst was filtered through a bed of Celite, washed with water (4 × 15 mL), and concentrated to provide a dark green solid. Recrystallization from hot ethanol furnished the pure desired product.

**2-(3,4-Diaminophenyl)-5-imidazolinobenzimidazole (17a):** 0.89 g (90%); mp 248−250 °C; $^1$H NMR (ppm) 4.0 (s, 4 H), 6.92 (d, 1 H, $J$ = 9 Hz), 7.74−7.93 (m, 4 H), 8.35 (s, 1 H), 10.8 (s 2 H). Anal. for $C_{16}H_{16}N_6$·2HCl·3$H_2O$, C, H, N.

**2-(3,4-Diaminophenyl)-5-amidinobenzimidazole (17b):** 0.990 g (88%); mp 280−282 °C; $^1$H NMR (ppm) 6.9 (d, 1 H), 7.71−7.84 (m, 4 H), 8.12 (s, 1 H), 9.17 (s, 2 H), 9.44 (s, 2 H). Anal. for $C_{14}H_{18}N_6$·2HCl·2$H_2O$, C, H, N.

**Preparation of 8−10.** To a well-stirred solution of the appropriate diamine (**17a** or **17b**, 3.70 mmol) in 4 N HCl (140 mL) was added the appropriate diacid (1.85 mmol). The solution was heated to reflux for 1 week and then concentrated to provide a dark green solid. Repeated recrystallization from hot ethanol provided the pure desired product.

**1,2-Bis[5-(5′-(2-imidazolinyl)-2′-benzimidazolyl)-2-benzimidazolyl]ethane (8):** 1.44 g (17%); mp 340−342 °C; FAB-MS $m/z$ 631 ($MH^+$ of free base); $^1$H NMR (DMSO-$d_6$ + NaOD) (ppm) 3.14 (s, 4 H), 3.62 (s, 8 H), 7.25−7.95 (m, 12 H), 8.2 (s, 2 H). Anal. for $C_{36}H_{30}N_{12}$·6HCl·2.5$H_2O$·0.5$C_2H_5OH$, C, H, N.

**1,2-Bis[5-(5′-(2-amidino)-2′-benzimidazolyl)-2-benzimidazolyl]butane (9):** 0.89 g (25%); mp >325 °C; FAB-MS 607 ($MH^+$ of free base); $^1$H NMR (ppm) 2.08 (s, 4 H), 3.30 (s, 4 H), 7.74−7.87 (m, 4 H), 7.98−8.05 (m, 4 H), 8.22 (2s, 2 H), 8.52 (d, 2 H, $J$ = 8 Hz), 8.78 (bs, 2 H), 9.16 (s, 2 H), 9.46 (s, 2 H). Anal. for $C_{34}H_{30}N_{12}$·6HCl·$H_2O$·1.9$C_2H_5OH$, C, H, N.

**1,2-Bis[5-(5′-(2-imidazolinyl)-2′-benzimidazolyl)-2-benzimidazolyl]butane (10):** 1.0 g (30%); mp 325 °C; FAB-MS 659 ($MH^+$ for free base); $^1$H NMR (ppm) 2.09 (s, 4 H), 3.31 (s, 4 H), 4.03 (s, 8 H), 7.78−8.0 (m, 8 H), 8.40−8.50 (m, 4 H), 8.73 (s, 2 H), 10.71 (s, 4 H). Anal. for $C_{38}H_{34}N_{12}$·6HCl·$H_2O$·0.5$C_2H_5$-OH, C, H, N.

**Buffer.** MES buffer contained 0.01 M MES 1 × $10^{-3}$ M EDTA. Sodium chloride was added to adjust the ionic strength, and the pH was adjusted to 6.2 with NaOH.

**DNA and RNA.** The polymers poly(dA)·poly(dT), polyd(A-T)$_2$ (Pharmacia), and poly(A)·poly(U) (Sigma) were prepared as previously described.[36] The oligomers d(GCGCGCGC), d(GCGAATTCGC), and d(CGCGAATTCGCG) (Midland Certified Reagent Co.) were purified by HPLC. The concentrations were determined optically using extinction coefficients per mole of strand at 260 nm determined by the nearest neighbor procedure.[37] For NMR, 1 mmol of DNA duplex solution was added to 0.5 mL of 7.5 mM sodium phosphate, 100 mM NaCl,

and 100 mM EDTA, pH 7.0, in an NMR tube. The $H_2O$ was removed under $N_2$ and the sample rehydrated in 0.5 mL of 99.996% $D_2O$ (Isotec). This removal of solvent and rehydration with $D_2O$ was repeated two times. The final solution was 2 mM in GCGAATTCGC duplex.

**DNA and RNA Thermal Melting.** Thermal melting experiments were conducted with Cary 3 or Cary 4 spectrophotometers interfaced to microcomputers as previously described.[38] A thermistor fixed into a reference cuvette was used to monitor the temperature. The DNA or RNA were added to 1 mL of buffer (MES with 0.1 M NaCl added) in 1 cm path length reduced volume quartz cells, and the concentration was determined by measuring the absorbance at 260 nm. Experiments were generally conducted at a concentration of $5 \times 10^{-5}$ M base pairs for the poly(dA)·poly(dT) and poly(A)·poly(U), and $3 \times 10^{-6}$ M in duplex for $d(G\text{-}C)_4$ and $d(CGCGAATTCGCG)_2$. For the complex $T_m$ experiments a ratio of 0.6 compound per base pair for poly(dA)·poly(dT), poly(A)·poly(U), and $d(G\text{-}C)_4$ and a ratio of one compound per oligomer duplex for $d(CGCGAATTCGCG)_2$ were used.

**Absorption Spectroscopy.** UV−vis scans were obtained as previously described[36,39] with Cary 3 or Cary 4 spectrophotometers in MES with 0.1 M NaCl added. Difference spectra were obtained by addition of the same amount of DNA to the sample cell and reference cell to subtract the DNA absorbance.

**Circular Dichroism.** CD spectra were obtained on a JASCO J-710 spectrometer interfaced to an IBM-PC computer. The software supplied by JASCO provided instrument control, data acquisition, and manipulation. Solutions of the compounds in MES buffer at 25 °C were scanned in 1 cm quartz cuvettes. A solution of the DNA was scanned, and the compound was then added and the sample rescanned at all desired ratios.

**Ethidium Displacement Experiments.** Ethidium bromide was added to 3 mL of MES buffer to give a concentration of $1.3 \times 10^{-6}$ M. DNA was added to the ethidium solution at a concentration of $1.8 \times 10^{-6}$ M in base pairs, and the maximum fluorescence was measured with an SLM 8000 spectrofluorometer at an excitation wavelength of 546 nm and an emission wavelength of 600 nm. Aliquots of a compound stock solution were added to the DNA−ethidium solution, and fluorescence was measured after each addition until greater than a 50% reduction of fluorescence was obtained. The apparent binding constant was calculated as previously described[40−43] by using the concentration of drug that gave a 50% reduction of the maximum fluorescence of the DNA−ethidium complex.

**Kinetics.** Kinetics measurements were conducted on a Hi-Tech SF-51 stopped-flow spectrometer interfaced to an HP 330 computer as previously described.[4,44] The SF-51 is equipped with a micromixing chamber and microcell that allow use of less than 50 mL of sample solution in each mixing event. Single wavelength kinetic records of absorbance or fluorescence versus time were collected.

**NMR Experiments.** Compound **5** was dissolved in 99.96% $D_2O$ (Isotec) to a concentration of 20 mM. For the 2:1 ratio of DNA duplex to ligand 0.5 mmol of compound **5** solution was added to the DNA duplex solution in the NMR tube. The solvent was removed under $N_2$ and 0.5 mL of 99.996% $D_2O$ added. For the 1:1 ratio sample an additional 0.5 mmol of compound **5** solution was added to the 2:1 sample, solvent was removed, and the sample was rehydrated with 0.5 mL of 99.996% $D_2O$. For the NMR of the uncomplexed compound **5**, 1 mmol of solution was added to 0.5 mL of the phosphate buffer solution, the solvent was removed, and the sample was rehydrated with 0.5 mL of 99.996% $D_2O$. The removal of solvent and rehydration with $D_2O$ was repeated two times to minimize the amount of HDO. All of the 1D and 2D $^1H$ spectra were collected on Varian spectrometers and the data transferred to a Silicon Graphics workstation for processing with the software package Felix (v2.30, Biosym). A 1D temperature study (data not shown) indicated that 35 °C is the optimal temperature for minimal signal overlap. The one-dimensional experiments were obtained with a spectral width of 4500 Hz, 16000 complex data points, a 1-s relaxation delay, and 100−500 transients. The residual HDO peak was used as an internal reference. The two-dimensional experiments were obtained with a spectral width of 3000 Hz in both dimensions with 1024 complex data points in the $t_2$ dimension and 512 points in the $t_1$ dimension (256 complex points in $t_1$ for the uncomplexed oligomer). Phase sensitive NOESY spectra were obtained with a mixing time of 350 ms using the method of States.[45]

**Molecular Mechanics and Modeling.** All models were built and energy minimized using the software package Sybyl (v6.03, Tripos). The Kollman all-atom forcefield[46,47] was used with minor modifications.[48] To better approximate the torsional barrier of biphenyl and related unfused aromatic compounds, some modifications were made to the forcefield of Veal and Wilson.[48] The HA (aromatic protons) van der Waals parameters were changed from $r^* = 1.30$ and $e = 0.0125$ to $r^* = 1.35$ and $e = 0.025$. Additionally, an explicit torsional term was added for CA−CA−CA−CA with $V_2/2 = 2.0$ and $V_2/2$ for *−CA−CA−* was raised from 2.65 to 3.75 (where CA is an aromatic carbon atom type). The combination of these three changes retain the *N*,*N*-dimethyluracil stacking and benzene−benzene interaction results of Veal and Wilson[48] while also giving a better description of the biphenyl torsional barrier.

The X-ray coordinates of the pentamidine complex with $d(CGCGAATTCGCG)_2$[16] were from the Brookhaven Protein Databank (PDB file 1D64) were used as a starting point for the DNA structure. The terminal CG base pairs of this dodecamer were removed and the ends capped with 5′- and 3′-OH groups. Compound **5** was built using the fragment library of Sybyl and the geometry optimized in an extended conformation using MNDO charges. This model was then visually docked into the pentamidine binding site of the DNA and the pentamidine was deleted. For the initial geometry optimization of this complex, the DNA was treated as an aggregate in Sybyl and the three NMR cross peaks between the ligand and DNA were used as symmetric range constraints (2−4 Å, 25 kcal/mol force constant). This complex was then energy minimized to a rms gradient of 0.08 kcal/(mol Å) using the Powell method. The aggregate on the DNA was removed and the complex energy minimized to a rms gradient of 0.08 kcal/(mol Å). Finally, the constraints were removed and the complex energy minimized to a rms gradient of 0.05 kcal/(mol Å), followed by minimization to a rms gradient of 0.02 kcal/(mol Å) using the BFGS method in SYBYL.

**Acknowledgment.** This research was supported by NIH Grant AI-33363. The NMR, UV−visible, and CD instruments were purchased through funds from NSF and the Georgia Research Alliance.

## References

(1) Zimmer, C.; Wahnert, U. Nonintercalating DNA-binding ligands: specificity of the interaction and their use at tools in biophysical, biochemical and biological investigations of the genetic material. *Prog. Biophys. Mol. Biol.* **1986**, *47*, 31−112.
(2) Pjura, P. E.; Grzeskowiak, K.; Dickerson, R. E. Binding of Hoechst 33258 to the minor groove of B-DNA. *J. Mol. Biol.* **1987**, *197*, 257−271.
(3) Wilson, W. D. Reversible Interactions of Small Molecules with Nucleic Acids. *Nucleic Acids in Chemistry and Biology*; Blackburn, G. M., Gait, M. J., Eds.; IRL Press: Oxford, 1993; Chapter 8, pp 295−336.
(4) Wilson, W. D.; Tanious, F. A.; Barton, H. J.; Jones, R. L.; Fox, K.; Wydra, R. L.; Strekowski, L. DNA Sequence dependent binding modes of 4′,6-diamidino-2-phenylindole (DAPI). *Biochemistry* **1990**, *29*, 8452−8461.
(5) Wilson, W. D.; Tanious, F. A.; Buczak, H.; Ratmeyer, L.; Venkatramanan, M. K.; Kumar, A.; Boykin, D. W.; Munson, R. Molecular Factors that Control the Nucleic Acid Binding Mode Selection by Unfused Aromatic Cations. *Structure & Function: Nucleic Acids*; Sarma, R. H., Sarma, M. H., Eds.; Adenine Press: Schenectady, NY, 1992; Vol. 1, pp 83−105.
(6) Coll, M.; Frederick, C. A.; Wang, A. H.-J.; Rich, A. A bifurcated hydrogen-bonded conformation in the d(A.T) base pairs of the DNA dodecamer d(CGCAATTGCG) and its complex with distamycin. *Proc. Natl. Acad. Sci. USA.* **1987**, *84*, 8385−8389.
(7) Kopka, M. L.; Pjura, P.; Yoon, C.; Goodsell, D.; Dickerson, R. E. *Structure and Motion: Membranes, Nucleic Acids and Proteins*; Clementi E., Corongiu, G., Sarma, M. H., Sarma, R., Eds.; Adenine Press: New York, 1985; pp 461ff.

(8) Kopka, M. L.; Yoon, C.; Goodsell, D.; Pjura, P.; Dickerson, R. E. The molecular origin of DNA-drug specificity in netropsin and distamycin. *Proc. Natl. Acad. Sci. U.S.A.* **1985**, *82*, 1376−1380.
(9) Kopka, M. L.; Yoon, C.; Goodsell, D.; Pjura, P.; Dickerson, R. E. Binding of an antitumor drug to DNA. Netropsin and d(CGC-GAATT$^{Br}$CGCG). *J. Mol. Biol.* **1985**, *183*, 553−563.
(10) Kopka, M. L.; Larsen, T. A. In *Nucleic Acid Targeted Drug Design*; Propst, C. L., Perun, T. J., Eds.; Marcel Dekker, Inc.: New York, 1992; pp 303−374.
(11) Niedt, G. W.; Schinella, R. A. *Arch. Pathol. Lab. Med.* **1985**, *109*, 727−734.
(12) Moskowitz, L.; Hensley, G. T.; Chan, J. C.; Adams, K. *Arch. Pathol. Lab. Med.* **1985**, *109*, 735−738.
(13) Bell, C. A.; Dykstra, C. C.; Aiman, N. A. I.; Cory, M.; Fairley, T. A.; Tidwell, R. R. Structure-Activity Studies of Dicationically Substituted Bis-Benzimidazoles against *Giardia lamblia*: Correlation of Antigiardial Activity with DNA Binding Affinity and Giardial Topoisomerase II Inhibition. *Antimicrob. Agents Chemother.* **1993**, *37*, 2668−2673.
(14) Bell, C. A.; Cory, M.; Fairley, T. A.; Hall, J. E.; Tidwell, R. R. Structure-Activity Relationships of Pentamidine Analogs against Giardia Lamblia and Correlation of Antigiardial Activity with DNA-Binding Affinity. *Antimicrob. Agents Chemother.* **1991**, *35*, 1099−1107.
(15) Dykstra, C. C.; Tidwell, R. R. Inhibition of topoisomerases from *Pneumocystis carinii* by aromatic dicationic molecules. *J. Protozool.* **1991**, *38*, 78S−81S.
(16) Edwards, K. J.; Jenkins, T. C.; Nedidle, S. Crystal Structure of a Pentamidine Oligonucleotide Complex: Implications for DNA-Binding Properties. *Biochemistry* **1992**, *31*, 7104−7109.
(17) Fairley, T. A.; Tidwell, R. R.; Donkor, I.; Naiman, N. A.; Ohemeng, K. A.; Lombardy, R. J.; Bentley, J. A.; Cory, M. Structure, DNA minor groove binding, and base pair specificity of alkyl- and aryl-linked bis(amidinobenzimidazoles) and bis-(amidinoindoles). *J. Med. Chem.* **1993**, *36*, 1746−1753.
(18) Tidwell, R. R.; Geratz, J. D.; Dann, O.; Volz, G.; Zeh, D. Diarylamidine Derivatives with One or Both of the Aryl Moieties Consisting of an Indole or Indole-like Ring. Inhibitiors of Arginine-Specific Esteroproteases. *J. Med. Chem.* **1978**, *21*, 613−623.
(19) Boykin, D. W.; Kumar, A.; Spychala, J.; Zhou, M.; Lombardy, R. J.; Wilson, W. D.; Dykstra, C. C.; Jones, S. K.; Hall, J. E.; Tidwell, R. R.; Laughton, C.; Nunn, C. M.; Neidle, S. Dicationic Diarylfurans as Anti-Pnemocystis carinii Agents. *J. Med. Chem.* **1995**, *38*, 912−916.
(20) Tidwell, R. R.; Jones, S. K.; Naiman, N. A.; Berger, I. C.; Brake, W. R.; Dykstra, C. C.; Hall, J. E. Activity of ctionically substituted bis-benzimidazoles against experimental Pneumocystis carinii pneumonia. *Antimicrob. Agents Chemother.* **1993**, *37*, 1713−1716.
(21) Dykstra, C. C.; McClernon, D. R.; Elwell, L. P.; Tidwell, R. R. SelectiveInhibition of Topoisomerases from Pneumocystis carinii Compared with That of Topoisomerases from Mammalian Cells. *Antimicrob. Agents Chemother.* **1994**, *38*, 1890−1898.
(22) Kumar, S.; Kansal, V. K.; Bhaduri, A. P. Possible Anthelmintic Agents : Synthesis of Ethyl 5(6)-[5(6)-Substituted-2-benzimidazolyl]benzimidazole-2-carbamates and Ethyl 4, 6-Dinitro-5-substituted-amino-benzimidazole-2-carbamates. *Indian J. Chem.* **1981**, *20B*, 254−256.
(23) Pinner, A.; Klein, F. Umwandlung der nitrile in imide. (Conversion of nitriles to imides.) *Chem. Ber.* **1887**, *10*, 1889−1897.
(24) Phillips, A. M. The Formation of 2-Substituted Benzimidazoles. *J. Chem. Soc.* **1928**, 2393−2399.
(25) Holan, G.; Evans, J. J.; Linton, M. Formation of Benzimidazoles at High Pressure. *J. Chem. Soc., Perkin Trans. 1* **1977**, 1200−1203.
(26) Morgan, K. J.; Turner, A. M. Studies in Heterocyclic Chemistry. III. *Tetrahedron* **1969**, *25*, 915−927.
(27) Crothers, D. M. Statistical thermodynamics of nucleic acid melting transitions with coupled binding equilibria. *Biopolymers* **1971**, *10*, 2147−2160.
(28) Wilson, W. D.; Tannious, F. A.; Buczak, H.; Venkatramanan, M. K.; Das, B. P.; Boykin, D. W. The effects of ligand structure on binding mode and specificity in the interaction of unfused aromatic cations with DNA. In Molecular Basis of Specificity in Nucleic Acid-Drug Interactions: *Jerusalem Symposia on Quantum Chemistry and Biochemistry*; Pullman, B., Jortner, J., Eds.; Kluwer Academic Publishers: Printed in the Netherlands, 1990; Vol. 23, pp 331−353.
(29) Hare, D. R.; Wemmer, D. E.; Chou, S. H.; Drobny, G.; Reid, B. R. *J. Mol. Biol.* **1983**, *171*, 319−336.
(30) Klevit, R. E.; Wemmer, D. E.; Reid, B. R. $^1$H NMR Studies on the Interaction between Distamycin A and a Symmetrical DNA Dodecamer. *Biochemistry* **1986**, *25*, 3296−3303.
(31) Lane, A. N.; Jenkins, T. C.; Brown, T.; Neidle, S. Interaction of berenil with EcoRI dodecamer d(CGCGAATTCGCG)$_2$ in solution studied by NMR. *Biochemistry* **1991**, *30*, 1372−1385.
(32) Larsen, T. A.; Goodsell, D. S.; Cascio, D.; Grzeskowiak, K.; Dickerson, R. E. The structure of DAPI bound to DNA. *J. Biomol. Struct. Dynam.* **1989**, *7*, 477−491.
(33) Wilson, W. D.; Tanious, F. A. Kinetic Analysis of Drug-Nucleic Acid Binding Modes: Absolute Rates and Effects of Salt Concentration. *Molecular Aspects of Anticancer Drug-DNA Interactions. Topics in Molecular and Structural Biology*; Neidle, S., Waring, M. J., Eds.; The Macmillan Press Ltd.: London, 1994; Vol. 2, pp 243−269.
(34) Saenger, W. *Principles of Nucleic Acid Structure*; Cator, C. R., Ed.; Springer-Verlag: New York, 1984; pp 220−282.
(35) Arnett, C. D.; Wright, J.; Zenker, N. Synthesis and Adrenergic Activity of Benzimidazole Bioisoesters of Norepinephrine and Isoproterenol. *J. Med. Chem.* **1978**, *21*, 72−78.
(36) Wilson, W. D.; Wang, Y.-H.; Kusuma, S.; Chandrasekaran, S.; Yang, N. C.; Boykin, D. W. Binding Strength and Specificity in DNA Interactions: The Design of A◊T Specific Intercalators. *J. Am. Chem. Soc.* **1985**, *107*, 4989.
(37) Fasman, G. D. Nucleic Acids. *Handbook of Biochemistry and Molecular Biology*, 3rd ed.; CRC Press: Cleveland, OH, 1975; Vol. 1, p 589.
(38) Kibler-Herzog, L.; Kell, B.; Zon, G.; Shinozuka, K.; Mizan, S.; Wilson, W. D. Sequence Dependant Effects in Methylphosphonate Deoxyribonucleotide Double and Triple Helical Complexes. *Nucleic Acids Res.* **1990**, *18*, 3545−3555.
(39) Wilson, W. D.; Lopp, I. G. Analysis of Cooperativity and Ion Effects in the Interaction of Quinacrine with DNA. *Biopolymers* **1979**, *18*, 3025−3041.
(40) Morgan, A. R.; Lee, J. S.; Pulleyblank, D. F.; Murray, N. L.; Evans, D. H. Ethidium fluorescence assays, Pari 1, Physiochemical studies. *Nucleic Acids Res.* **1979**, *7*, 547−569.
(41) Debart, F.; Perigaud, C.; Gosselin, G.; Mrani, D.; Rayner, B.; LeBer, P.; Auclair, C.; Balzarini, J.; DeClercq, E.; Paoletti, C.; Imbach., J.-L. Synthesis, DNA binding, and biological evalution of synthetic precursors and novel analogues of netropsin. *J. Med. Chem.* **1989**, *32*, 1074−1083.
(42) Lee, M.; Rhodes, A. L.; Wyatt, M. D.; Forrow, S.; Hartley, J. A. GC Base Recognition by Olig(imidazolecarboxamide) and C-Terminus-Modified Analogues of Distamycin Deduced from Circular Dichroism, Proton Nuclear Magnetic Resonance, and Methidiumpropylethylenediaminetetraacetate-Iron(II) Footprinting Studies. *Biochemistry* **1993**, *32*, 4237−4245.
(43) Lee, M.; Rhodes, A. L.; Wyatt, M. D.; Forrow, S.; Hartley, J. A. Design, synthesis, and biological evaluation of DNA sequence and minor groove selective alkylating agents. *Anti-Cancer Drug Des.* **1993**, *8*, 173−192.
(44) Tanious, F. A.; Yen, S.-F.; Wilson, W. D. Kinetic and equilibrium analysis of a threading intercalation mode: DNA sequence and ion effects. *Biochemistry* **1991**, *30*, 1813−1819.
(45) States, D. J.; Haberkorn, R. A.; Ruben, D. J. A Two-Dimensional Nuclear Overhauser Experiment with Pure Absorption Phase in Four Quadrants. *J. Magn. Reson.* **1982**, *48*, 286−292.
(46) Weiner, S. J.; Kollman, P. A.; Case, D. A.; Singh, U. C.; Ghio, C.; Alagona, G.; Profeta, S., Jr.; Weiner, P. A new force field for molecular simulation of nucleic acids and proteins. *J. Am. Chem. Soc.* **1984**, *106*, 765−784.
(47) Weiner, S. J.; Kollman, P. A.; Nguyen, D. T.; Case, D. A. An all atom force field for simulations of proteins and nucleic acids. *J. Comput. Chem.* **1986**, *7*, 230−252.
(48) Veal, J. M.; Wilson, W. D. Modeling of Nucleic Acids Complexes with Cationic Ligands: A Specialized Molecular Mechanics Force Field an Its Application. *J. Biomol. Struct. Dynam.* **1991**, *8*, 1119−1145.

JM9507946